Journal of Thermal Analysis and Calorimetry
https://doi.org/10.1007/s10973-026-15335-4

Comparative analysis of hybrid modelling for performance and emissions using biodiesel with nanoadditives and hydroxy

M. S. Gad[1] · Ahmed Alenany[2,3,4] · Ahmed M. Helmi[4,2]

Received: 30 July 2025 / Accepted: 11 January 2026

Abstract

Fossil fuels provide the majority of the world's energy needs. When fossil fuels are burned, harmful pollutants have negative impacts on the environment. It is advantageous to use biodiesel in diesel engines. Nanoadditives were employed to enhance the characteristics and usage of biodiesel in cold regions. Diesel was mixed with 20% WCO biodiesel. Distribution of cerium and titanium oxides in B20 was 25 and 50 parts per million. Using an alkaline electrolyser, water was electrolysed at a rate of 0.5 litre per minute to produce hydroxy gas. Influence of methyl ester blend containing hydroxy gas and nanomaterials on emissions and engine performance was investigated. The largest declines in specific fuel consumption were 15 and 20%, whereas cerium and titanium oxides at 50 ppm with hydroxy demonstrated increases in thermal efficiency of 14 and 19% when related to B20. When 50 ppm of cerium and titanium oxides with hydroxy were added, the biggest reductions in smoke were 15% and 21%, respectively, while the biggest decreases in NOx emissions were 24% and 35% for B20 + 50C + HHO and B20 + 50T + HHO, respectively. For titanium and cerium oxides with hydroxy, CO concentrations were reduced by 13% and 20%, respectively, whereas HC was declined by 25% and 36%. ANN and linear regression methods were utilised to model emissions and performance. For all variables, ANN and regression fared better, with R^2 values above 0.97. For more ecologically friendly and effective engine operation, B20 with 50 ppm cerium and titanium oxides with hydroxy is advised.

Keywords Biodiesel · CeO_2 · TiO_2 · HHO · Performance · Emissions · Modelling

Abbreviations

ANN	Artificial neural network
ASTM	American Society of Testing and Materials
B20	Biodiesel blend (20% biodiesel + 80% diesel oil)
BSFC	Brake specific fuel consumption, kg/kW.hr
BTE	Brake thermal efficiency, %
CO	Carbon monoxide concentrations, %
D100	Pure diesel oil
EGT	Temperature of exhaust gases, °C
HC	Hydrocarbon emission, ppm
HHO	Hydroxy (oxyhydrogen) gas.
NOx	Nitrogen oxides emission, ppm
KOH	Potassium hydroxide
LPM	Litre per minute
MRAE	Mean relative absolute error
MAPE	Mean absolute percentage error
ppm	Part per million
R^2	Coefficient of correlation
WCO	Waste cooking oil
SEM	Scanning electron microscope
TEM	Transmission electron microscope

✉ M. S. Gad
msm19@fayoum.edu.eg

[1] Mechanical Engineering Department, Faculty of Engineering, Fayoum University, Fayoum, Egypt

[2] Department of Computer and Systems Engineering, Faculty of Engineering, Zagazig University, Zagazig 44519, Egypt

[3] Department of Computer Systems Engineering, October University for Modern Sciences and Arts (MSA University), Giza 12451, Egypt

[4] Computer Engineering Department, College of Engineering and Information Technology, Buraydah Private Colleges, 51418 Buraydah, Saudi Arabia

Introduction

Internal combustion engines using traditional fossil fuels are currently the primary suppliers of electricity and transportation. Diesel engines in particular are widely used in power generation because of their inherent benefits, which include efficiency and high power-to-mass ratios. By 2050, non-renewable and limited petroleum supplies will be

Published online: 06 March 2026

depleted, according to US Energy Information Administration (EIA) projections [1]. Scientists should work to lower the exhaust emissions from diesel engines, which include smoke, unburned hydrocarbons, CO, particulate matter, and NOx. These pollutants are harmful to both human health and the environment [2]. Engine pollution regulations are getting stricter every year. Because of this, scientists are pushed to look at ways to reduce emissions and develop cleaner, renewable fuels that don't require engine modifications, as well as more environmentally friendly alternatives [3]. Fossil fuels could be completely replaced by biofuels and other sustainable alternative energy sources. Among various benefits they provide are regional growth, reduced greenhouse gas emissions, renewable energy, long-term sustainability, and others [4]. Because it has fuel characteristics near to those of diesel fuel and can be used with very minimum engine modifications, biodiesel stands out among all other biofuels [5]. Because it is sulphur-free, oxygenated, sustainable, high flash point, biodegradable, emits fewer emissions, and can be made from range of feedstocks, including waste, vegetable, algae-derived, and microbial oils, as well as animal fats, biodiesel has the following advantages over pure diesel [6]. Using biodiesel has several disadvantages despite these advantages. Some of the main drawbacks include poor cold and spray characteristics, increased viscosity, lower calorific value, elevated NOx levels, engine power losses, and BSFC increase [7, 8]. As mentioned before, low fuel economy, poor atomisation, and cold starting issues are the primary issues with methyl ester fuel. Nanomaterials are frequently used as additives to improve engine performance and emission characteristics [9–11]. Metal based of low pour point, high flash point, oxygen content, anti-oxidation, and high cetane number are some ways to improve methyl ester properties [12].

Due to its sustainability, lack of sulphur, and lower emissions of pollutants, biodiesel is regarded as one of the best diesel substitutes. The vital challenge to the widespread application of biodiesel is its high cost in comparison with conventional diesel fuel. Waste cooking oil (WCO) is the most cost-effective source of biodiesel fuel due to its low cost. To enhance engine performance, emissions, and combustion properties, nanoparticles were introduced. Because of its quick vaporisation and short ignition delay, biodiesel combination with nanoadditives has higher cylinder pressure and heat release rate than B20. Inclusion of nano-TiO_2 to biodiesel resulted in 22.57% reduction in NOx emissions compared to pure biodiesel. Blending biodiesel mixture with 25 ppm concentration of nano titanium oxide resulted in 16.25% reduction in smoke emissions [13]. When nano-TiO_2 with mass concentration of 25 ppm was introduced, BTE was increased by 24.94% compared to alumina with the same dose. When nano-TiO_2 and Al_2O_3 were blended, the ignition delay period was decreased by 0.99 and 5.47%, respectively, related to basic fuel [14]. When TiO_2 nanoparticles were blended with palm biodiesel, the thermal efficiency was increased in comparison with pure biodiesel. The use of the nanomaterial resulted in improvements in emissions levels and combustion characteristics [15]. Tamanu biodiesel B30 was mixed with nano titanium oxide at percentages of 25, 50, and 100 ppm. Because of the better fuel properties, there were reductions in HC, CO, NOx, and smoke emissions as compared to B30 [16, 17]. The addition of nano titanium oxide to methyl ester mixture reduced the levels of smoke [18]. For crude diesel, carbon monoxide, hydrocarbons, and smoke were decreased at nano titanium oxide of 100 and 200 ppm. Because of the catalytic impact, increased oxidation capability, and higher thermal conductivity, addition of TiO_2 nanofluid to methyl ester resulted in emissions decreases [19]. Volume percentage of 40% Acacia Concinna biodiesel mixed with diesel oil with TiO_2 nanoparticles at dosages variations. Since BSFC, smoke, and HC were reduced by 18.42, 38, and 20%, respectively, in comparison with base fuel, the recommended amount of 150 mg/litre of TiO_2 was reached [20].

Urgent need for a new sustainable fuel that produces no pollution as a result of the depletion of fossil fuels and the sharp rise in pollution levels that follows is urgent. Brown gas HHO is a blend of hydrogen and oxygen that is created when water is electrolysed. Hydrogen has the highest calorific value and fastest flame speed. Performance and emissions of karanja biodiesel and diesel blends were improved with 0.73 litre per minute (LPM) flow rate of HHO as compared to diesel [21]. With the exception of NOx emissions, performance and emission outcomes are improved. When hydroxy gas was added to intake air instead of pure diesel fuel, encouraging results were obtained [22]. In relation to pure diesel, HHO gas's greater oxygen content results in higher combustion efficiency and improved performance. Using the high cell gap under the same electrolyte content and operating temperature circumstances resulted in greater rate of hydroxy. When compared to fuel without HHO, the optimal production condition with low fuel consumption and emissions was found to be an anode–cathode cell spacing of 10 mm. When hydroxy was added, CO emission was decreased by 8–12%, while NOx emissions rose. Performance and emissions were improved with HHO inclusion. The benefits of HHO include the additional oxygen, broad flammability range, high burning velocity, and lack of carbon [23]. Using biodiesel with HHO reduces CO, HC, and smoke emissions up to 50%, 40%, and 85%, respectively. CO_2 and NOx concentrations rose by up to 6% and 10%, respectively, when HHO gas was applied. The carbon oxidation was enhanced by the addition of hydrogen and oxygen. The rise in NOx emissions was caused by the high cylinder combustion temperature. Cylinder pressure was improved with HHO gas inclusion [24]. When HHO is used,

an average of 19.1% increase in engine torque was achieved. Application of HHO resulted in an average decrease in specific fuel consumption of 16.3%. With HHO flow rate of 2 LPM, 13.23% less diesel fuel was used. The longer engine oil life resulted in less carbon accumulation in the cylinder. At low engine load, specific fuel consumption was dropped by up to 20% [25].

Because HHO is more flammable, the temperature of the exhaust gas and NOx rose. Due to HHO improved properties than diesel oil, BTE was enhanced by 13.28%. Hydrogen in HHO caused about 6% boost in output power when compared to diesel oil. Using hydroxy gas decreased HC emission by an average of 33% and CO emissions by 23 %. There was an 8% decrease in smoke emissions compared to diesel oil. Enhanced combustion is made possible by the combined action of oxygen and hydrogen [26]. NaOH is used as a catalyst in dry cells to produce oxyhydrogen gas. Fuel consumption was reduced by 14.8%, reductions in CO and HC concentrations were 33% and 27.4%, respectively [27]. HHO electrolyser consists of double parallel connected dry cells with 14 plates, bubbler, water reservoir, current pulse width modulator, electrical wires and fittings. A battery of 24 V and 30 A was used as power supply to HHO generator to yield 10 LPM [28]. Using HHO resulted in average decreases of 13.5, 5, and 14% in CO, HC, and BSFC, respectively [29, 30]. The electrode material, geometrical parameters, electrolyte content, and current flow all affect the rate at which HHO gas is produced [31]. HHO cells come in two varieties as wet cells and dry cells. Because HHO dry cells are smaller and easier to install in engines, they were employed [32]. The HHO flow rate directly rises as the catalyst mass fraction in water increases. Because of its fast burning velocity, carbon-free content, and additional oxygen, HHO gas performed well and less emitted in engines [33–35].

Water was split into hydrogen at the cathode and oxygen at the anode using DC current. To separate water molecule, a voltage of about 1.23 V is required. HHO was produced using catalysts such as NaOH, KOH, and NaCl. KOH's superior electrical conductivity has led to its widespread application. An unstable form of H_2O vapour is called HHO [36, 37]. Because of its rapid burning velocity and low ignition energy, hydroxy fuel burned entirely at high flame speeds. Because of its short hydroxy quenching distance, rapid flame speed, and extended flammability range, the diesel fuel completely burnt under high-speed conditions [29]. Diesel engines were tested with hydroxy rates ranging from 1 to 3.3 LPM and under various loads. Electrolyte type (NaOH and KOH), electrode spacing (2 mm and 3 mm), electrode surface roughness (rough and smooth), and electrolyte concentration (20% and 30%) are the influencing factors [25, 36, 38]. When KOH was employed at 30% and rough electrodes were spaced 3 mm apart, stainless steel 316L electrodes performed well [39, 40]. A dry cell electrolyser produced 0.375 LPM of HHO gas. The amount of catalyst (NaOH), applied voltage, current, number, and area of electrodes and stacks were all examined [41–43]. Seven serial plates at the anode, 5% NaOH solution, and 3 mm gap made up the electrolyser. Flow rate of 1 LPM HHO was supplied in the engine air intake which reduced fuel consumption by 6–12% [44]. Emissions of smoke, CO, HC, and HC were dropped by 49%, 58, and 60 %, respectively. Increase in NO_X emissions was caused due to the oxygen content of HHO [45]. Enrichment of hydroxy increased the output power and decreased the specific fuel consumption [46].

By adding hydrogen to diesel engines, CO and hydrocarbon concentrations were declined, but brake thermal efficiency was improved [47]. Carbon nanotubes and titanium oxide nanomaterials are used in diesel engines to reduce brake-specific fuel consumption. Recent studies concentrate on the effects of combining tire oil with nano cerium oxide regarding emissions, combustion, and performance in diesel engines [48]. However, the impact of nanoadditives in conjunction with hydroxy gas on emissions and engine performance remains largely unexamined [45]. Nanoadditions show promise in improving heat transfer, promoting evaporation, and improving the thermal characteristics of base fuels. There are issues with the consistency of air–fuel mixing and combustion efficiency as a result of the restrictions on atomization and vaporisation of methyl ester [49]. Pyrolysis oil derived from discarded tires, compliant with ASTM standards, is recognised as a feasible energy source. The main focus of this work is how diesel engine emissions, combustion, and performance are affected by mixed tire oil containing nano cerium oxide [24].

According to this work, there is an undiscovered gap in the literature. The effects of biodiesel, nanoadditives, and hydroxy (HHO) enrichment on CI engine performance and emissions have been the subject of numerous experimental studies; however, thorough comparative studies that assess and validate hybrid modelling approaches for predicting these effects are conspicuously lacking. The literature study indicated that previous studies primarily focused on the impacts of biodiesel/diesel blends having a single nanomaterial addition, indicating a paucity of research on the effects of various nanomaterials at varied ratios on diesel engine performance and emissions. Specifically, it has not been extensively modelled utilising hybrid methodologies (ANN–regression) and benchmarked against experimental data with appropriate statistical validation and accurately forecasting on the joint influence of biodiesel–nanoadditive–HHO interactions on engine behaviour. Therefore, the objective of this research is to develop a model that minimises money, time, and labour losses. This study's main goal is to compare hybrid modelling techniques for forecasting engine performance and emission characteristics

when using biodiesel fuels supplemented with hydroxy and nanoadditives. The specific goals are to determine the predictive accuracy of various hybrid models under various operating conditions and evaluate their capacity to capture the combined effects of HHO enrichment and nanoadditive to determine the most dependable modelling framework for performance and emission prediction. Statistical validation criteria as R^2, MRAE, and MAPE were used compare the accuracy and robustness of the suggested models and compare their predicted performance to experimental findings.

Addition of nanocerium and titanium oxides improved the thermal properties of the base fuel. Issues with atomization and vaporization during biodiesel operation resulted in improper fuel–air mixing and insufficient combustion. This study reduces the negative effects of disposing of WCO and saves money by using non-edible oil that generates more biodiesel. It is possible to turn used cooking oil into usable energy. WCO was converted to methyl ester by transesterification process and mixed with diesel oil in 20% by volume. ASTM states that the properties of biodiesel and diesel combination are comparable to those of diesel oil. Biodiesel mixture B20 was supplemented with nanomaterials such as cerium and titanium oxides at varying concentrations of 25 and 50 parts per million. Hydroxy gas was produced from dry electrolyser and injected into the air intake at 0.5 litre per minute. This research compares two modelling approaches: linear regression and artificial neural network. The accuracy of the prediction model was shown by comparing the outputs of the modelling approach with the experimental findings. Thermal efficiency, specific fuel consumption, and exhaust gas temperature were used to assess engine performance. Exhaust concentrations, such as smoke, HC, CO, and NOx, have been studied. This work supports future waste-to-energy and low-carbon fuel applications in CI engines by developing modelling system that can accurately estimate performance and emission trends.

Methodology

Biodiesel conversion

Waste cooking oil is not used directly in diesel engines because of its increased viscosity and density. WCO was purified of pollutants and gums. WCO was preheated to 100 °C in order to eliminate the humidity. The oil is then transferred into a flask that is held up by condenser, magnetic stirrer, and thermometer. Methoxide was produced by mixing of 1:9 molar methanol with 1.5% by mass potassium hydroxide. WCO was transformed into methyl ester during the transesterification process. The oil and methoxide mixture was stirred for 90 min. at 60 °C to create methyl ester and glycerin. The mixture was left in the separating funnel for 12 hrs. to remove the glycerin and ester. The catalyst, impurities, and unreacted methanol are eliminated using warm water. A rotary evaporator was used to dry the biodiesel after the water was removed. Diesel oil and methyl ester were mixed in 20% volumetric ratio. The characteristics of crude diesel and biodiesel mixtures are listed in Table 1.

Pretreatment of biodiesel with nanoadditives

Nanotech, Egypt, provides cerium and titanium oxides, and its properties are shown in Table 2. Utilising transmission electron microscope (TEM) and scanning electron microscope (SEM), the surface and morphology of nanoadditives were investigated. SEM and TEM of nanoparticles are displayed in Figs. 1 and 2. B20 biodiesel blend was mixed with nanomaterials. To create the tested fuels, nanoparticles were added to the methyl ester mixture at mass fractions of 25 and 50 ppm as 0.0025 and 0.005% by volume, respectively. The purpose of selecting these concentrations is to eliminate the suspension and improve stability. Pulse rates were used in conjunction with magnetic stirring and ultrasonication to disperse the nanoadditives throughout the base fuel and avoid agglomeration. It took 45 min. of constant agitation to get the uniform dispersion. Blended methyl ester with

Table 2 Properties of nanoparticles

Properties	TiO_2	CeO_2
Manufacturer	Nanotech. company	
Appearance (colour)	White	White
Bulk density, gm cm^{-3}	0.24	0.53
Avg. size (TEM)	35 ± 5 nm	< 50 nm
Shape	Spherical	Spherical

Table 1 Properties of biodiesel and its mixtures

Properties	Method	Biodiesel WCO	B20	Diesel
Specific gravity @ 15 °C , kg m^{-3}	ASTM D- 4052	0.883	0.84	0.835
Kinematic viscosity @ 40 °C , cSt	ASTM D- 445	4.5	3.1	2.9
Flash point, °C	ASTM D- 93	120	82	72
Cetane number	ASTM D- 13	52	50	49
Calorific value, MJ kg^{-1}	ASTM D- 224	39.5	41.5	42

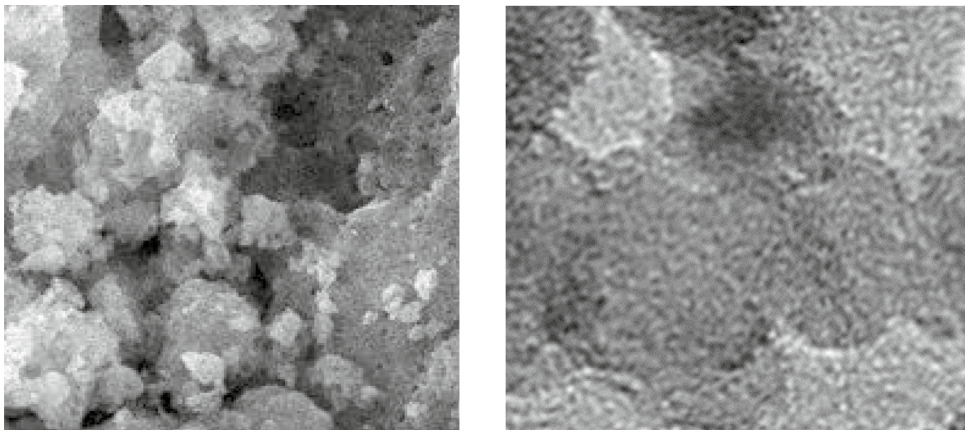

(a) SEM of nano CeO_2 **(b)** TEM of nano CeO_2

Fig. 1 SEM and TEM analysis of nanomaterial

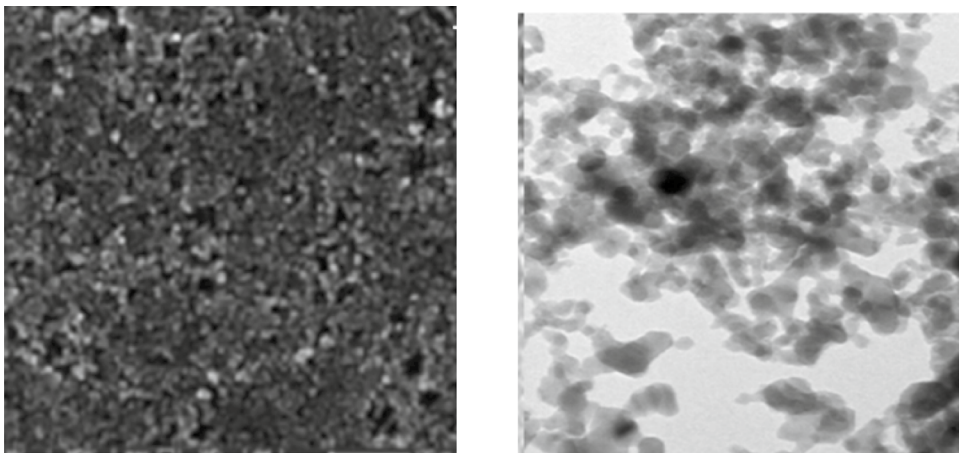

(a) SEM Photos of nano TiO_2 **(b)** TEM Photos of nano TiO_2

Fig. 2 Photographs of SEM and TEM for nanoadditive

nanoparticles should be administered immediately after preparation to prevent sedimentation. To get concentrations of 25 and 50 ppm, 0.025 and 0.05 g of each nanomaterial were added to 1 litre of the blend, respectively. B20 + 25T, B20 + 50T, B20 + 25C, and B20 + 50C were the names assigned to the biodiesel blend combinations that included TiO_2 and CeO_2 of 25 and 50 ppm, respectively. Surfactants like Span80 (1%) and Tween80 (1%) were employed to scatter the nanomaterials and increase the stability of the methyl ester mixture. To assess stability, a mixture of biodiesel and nanoparticles was kept in a long tube under static conditions for fifteen days to check the samples stability.

HHO production

The electrolyser configuration included parallel dry cell with pulse width modulation, electrical connections, solenoid relay, fittings, water reservoir, and bubbler. The cell was rectangular and measured as 250 × 200 mm. A flame arrestor was installed to eliminate the engine backfire. The dry cell was powered by 12V and 20A DC battery. Rectangular 316L stainless steel plates with clamped gaskets that allowed water to pass between them to build this specific dry cell. Hydroxy gas was generated by the nine-plate cell directed towards the bubbler. A constant 0.5 LPM of HHO was fed into the engine's air intake manifold. The used catalyst is KOH of 20% concentration. The HHO flow rate was determined by measuring the volume of water collected in the graduated reservoir over predetermined time. Dry HHO electrolyser is schematically illustrated in Fig. 3.

Experimental setup

The experiment used a four-stroke, air-cooled, and single-cylinder diesel engine that could provide up to 5.7 kW of power at 1500 rpm. The engine has 17.5:1 compression ratio, diameter

of 100 mm, and stroke of 105 mm. The test rig system's schematic description is displayed in Fig. 4. An AC generator with an electrical output of 10.5 kW that was directly linked to the engine to calculate the engine's brake output power. Output voltage and current data were used to determine how much electricity that the load bank consumed. To reduce the pulsing air flow, sharp edge orifice was placed at the side of the air box and used to compute the intake air flow. A U-tube manometer was used to evaluate the pressure drop across the orifice. Type K thermocouple was used to measure the temperatures of intake air and exhaust gas. Measurements were made of smoke and exhaust gas emissions as CO, HC, and NOx. Gas analyser (HC (0–2000 ppm), NO (0–4000 ppm), (O_2 (0–22%), CO_2 (0–10%), and NO_2 (0–1000 ppm)) was used with smoke meter (opacity 0-99% and resolution 0.1). Before the tests, the engine was first ran without load for 20 minutes to warm it up using diesel under steady state conditions to ensure the engine stability. Methyl ester mixture B20, which was blended with nanoparticles, was then used to power the engine. The engine was operated with range of loads and stable running speed of 1500 rpm at each measurement. Uncertainty analysis was used to assess data dependability and repeatability in order to guarantee statistical validity. For thermal efficiency, HC, NOx, CO, and smoke emissions, the largest degree of uncertainty was found at ±1 ppm, ±1 ppm, ±0.01% vol., ±1%, and ±1.5%, respectively. Engine speed, brake power, exhaust gas temperature, and specific fuel consumption were determined to have the highest measurement errors, at 0.2, 0.85, 0.2, 2.2, and 0.15 %, respectively. By summing up all of the parameter uncertainties, the overall uncertainty was calculated using the following formula.

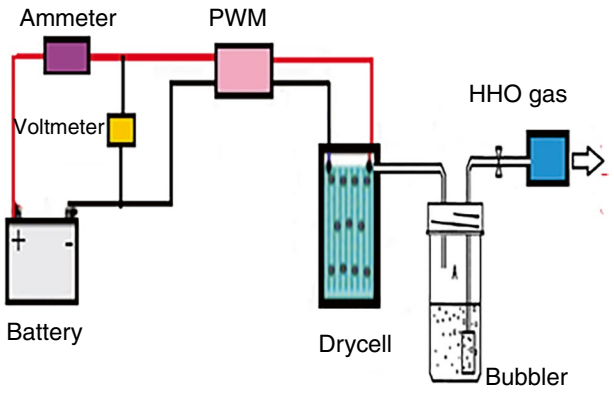

Fig. 3 Dry electrolyser schematic diagram

$$\sqrt{(ubp)^2 + (uTexh)^2 + (uN)^2 + (usfc)^2 + (uther)^2 + (uHC)^2 + (uCO)^2 + (uNOx)^2}$$
$$= \sqrt{(0.85)^2 + (0.2)^2 + (0.15)^2 + (2.2)^2 + (1.5)^2 + (0.01)^2 + (1)^2 + (0.2)^2 + (1)^2 + (1)^2} = \pm 3\%$$

where

Output load uncertainty is represented by ubp, EGT uncertainty by uTexh, engine speed uncertainty by uN, CO concentration uncertainty by uCO, HC emission uncertainty by uHC, BSFC uncertainty by usfc, BTE uncertainty by uther, and NOx uncertainty by uNOx.

Engine performance and emissions forecasting

It is useful to employ a mathematical model to predict engine performance and emissions because it can be expensive and time-consuming to set up tests for engine performance evaluation and track pollutants. Based on experimental input–output tests, this model employs various combinations of engine brake power and fuel blends. Three mathematical models were used to forecast the output variables: ANN and regression. These methods are reviewed in the section that follows.

Linear regression

Linear regression is the main technique used to model the relationship between two variables. When the relationship is not perfectly linear, regression can be used to increase the model's ability to predict the dependent variable accurately. Model is vulnerable to noise and outliers because even one or two outliers in the data might significantly impact it. On the other hand, the data can be piecewise linear. Tree models are appropriate options in this situation for capturing these intricate interactions between variables. Regression's primary benefits are its interpretability and transparency. The sum of squared residuals between the expected and actual outputs is minimised in order to train regression. After a thorough investigation, it can be realised that there is a nonlinear relationship between each of the seven variables and the engine load. Based on the aforementioned observation, the following linear regression model is proposed to describe the seven engine and emission variables as shown in Equation (1).

$$V = x_0 + x_1 L + x_2 L^2 + x_3 B + x_4 C + x_5 T + x_6 H \quad (1)$$

where V is a predicted dependent variables variable, L is the engine load, B is the biodiesel blend percentage (0 denotes 0% and 1 denotes 20%), C is the CeO_2 nanomaterial concentration (ppm), T is the TiO_2 nanomaterial concentration (ppm), and H denotes whether there is an HHO injection of 0.5 litre per minute. H is either 0 meaning no HHO flow or 1 if there is flow. Finally, the parameters $x_i, i = 0, 1, \ldots, 6$ are the model parameters to be estimated using least squares.

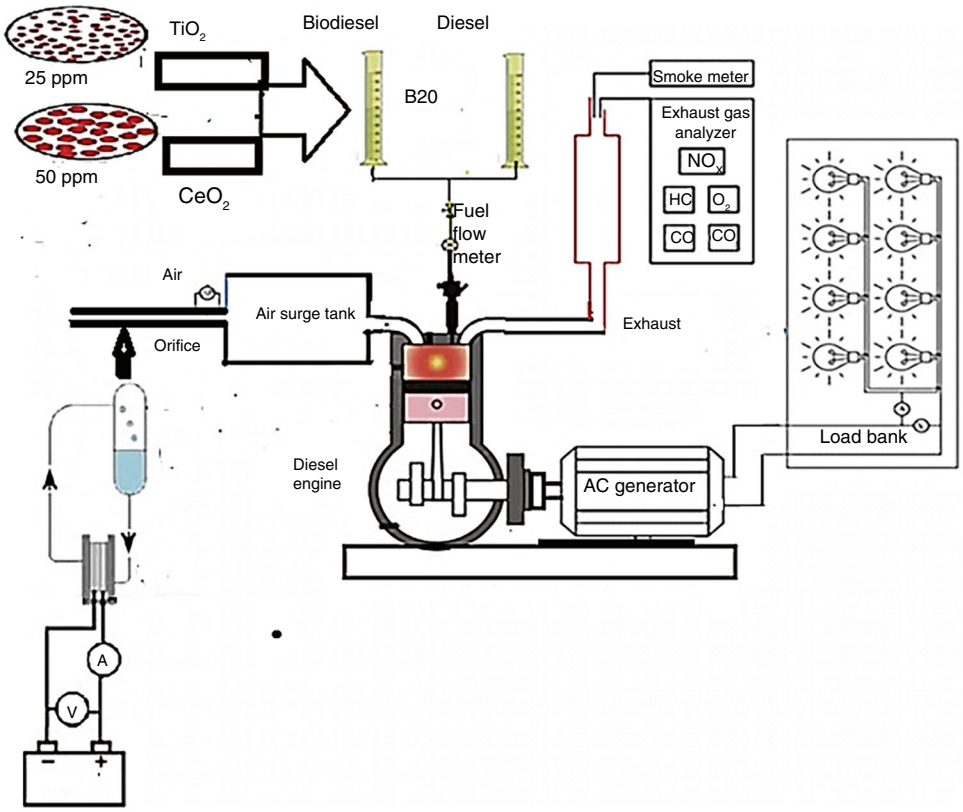

Fig. 4 Schematic diagram of test rig

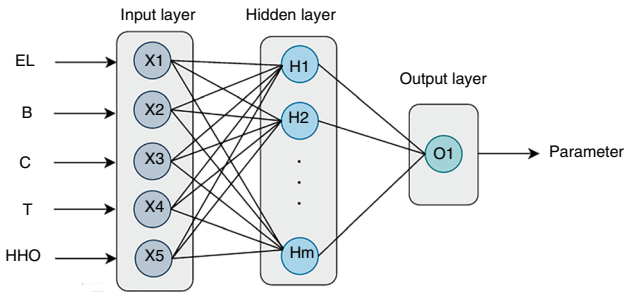

Fig. 5 ANN prediction model

For this purpose, data are split into 75% train and 25% test (for SFC) and 80%/20% for other variables. The least squares are performed and averaged over 1000 experiments. Applying linear regression, we arrive at the following parameter values as shown in Eq. (2).

$$\begin{pmatrix} SFC \\ TE \\ EGT \\ CO \\ HC \\ Nox \\ SE \end{pmatrix} = \begin{pmatrix} 0.879 & -1.546 & 0.100 & 0.090 & -0.007 & -0.034 & -0.045 \\ 1.632 & 60.547 & -38.432 & -3.407 & 0.907 & 1.659 & 1.250 \\ 139.035 & 101.038 & 47.251 & 50.425 & -7.469 & -20.509 & -20.040 \\ 0.027 & -0.016 & 0.035 & -0.001 & -0.001 & -0.004 & -0.004 \\ 17.197 & -0.452 & 16.003 & -3.635 & -2.198 & -4.537 & -4.437 \\ 19.573 & -13.315 & 113.472 & 48.609 & -10.262 & -19.312 & -20.593 \\ 13.667 & -3.827 & 39.692 & -1.884 & -1.385 & -4.647 & -4.316 \end{pmatrix} \begin{pmatrix} 1 \\ L \\ L^2 \\ B \\ C \\ T \\ H \end{pmatrix} \quad (2)$$

ANN technique

Inspired by the way biological neural networks develop artificial neural networks are a flexible machine learning algorithm. Layers of connected "neurons" that are "weighted" according to the kind of relationship are how an artificial neural network is represented. Before sending the output to the following layer, neurons receive inputs from the layer above, where a computation is made. An ANN model is designed with a structure (5-N_h-1), where there are five input factors in the conducted experimentation. N_h denotes the number of neurons in the hidden layer. The settings of this parameter are examined among the values 5, 7, 10, and 12 to determine the best ANN structure. Each output parameter in the experimentation has a separate ANN model as appears in Fig. 5. The testing strategy is randomly leave-one-sample-out of the examined category. ANN model is trained using Levenberg–Marquardt

backpropagation algorithm, the number of epochs is 1000 and the training rate is set to 0.01. The activation function of the hidden layer is a hyperbolic tangent sigmoid ("tansig") activation, while a pure line ("purelin") is used for the output layer. The average mean relative absolute error (MRAE) is defined in Eq. (3), over 25 independent computer runs.

$$MRAE = \frac{1}{N_t}\sum_{i=1}^{N_t}\frac{|y_i - O_i|}{y_i} \quad (3)$$

where N_t denotes the number of samples of test set, y_i is the target value of the i-th samples, and O_i is the corresponding output of the ANN.

The designed ANN for predicting the behaviour of output parameters is shown in Fig. 5. Inputs are: engine load (EL), (B), (C), (T), and (HHO). Output is one of the parameters: specific fuel consumption (gm kWh^{-1}), EGT (°C), BTE (%), CO emission (%), HC emission (ppm), and Nox emission (ppm). Input layer entries are denoted by (X), neurons in the hidden layer are denoted by (H), and the output neuron is denoted by (O).

Results and discussion

Brake specific fuel consumption (BSFC)

Figure 6 shows the impact of a biodiesel mixture containing CeO_2 and TiO_2 at 25 and 50 ppm with HHO on specific fuel consumption. Due to the improved combustion efficiency and decreased amount of fuel at high output power, the BSFC evaluations were declined as the load increased. Specific fuel consumption of biodiesel mixture is higher than crude diesel because of its lower calorific value about diesel oil and problems with fuel atomization caused by the methyl ester's increased density and viscosity. Owing to the enhanced atomization and combustion properties, the addition of nanoparticles to methyl ester reduced BSFC at all nanoparticle dosages in WCO biodiesel mixture. Secondary atomization of the nanoparticles results in the decrease in fuel usage. Better fuel/air mixing and reduced specific fuel consumption are the results of secondary atomisation and micro-explosion working together. Because of improved heat transfer and momentum exchange between the molecules of fuel, BSFC is lower than base fuel. Nanoadditives enhanced catalytic surface activity and accelerated the evaporation rate. It has been shown that cerium and titanium oxides' higher surface area-to-volume ratio, thermal conductivity, and oxygen-carrying functional groups result in specific fuel consumption decreases. Additionally, the influence assessment of adding cerium oxide revealed that the induction of hydroxy in the same output power range led to the decrease in BSFC when compared to its absence. Because of its improved fuel–air mixture, HHO's oxygen content promotes improved ignition and combustion [29]. BSFC was dropped as the result of higher Brown gas diffusivity. The BSFC of the studied fuels was reduced because hydroxy gas is more flammable and uses less fuel because of its quick flame

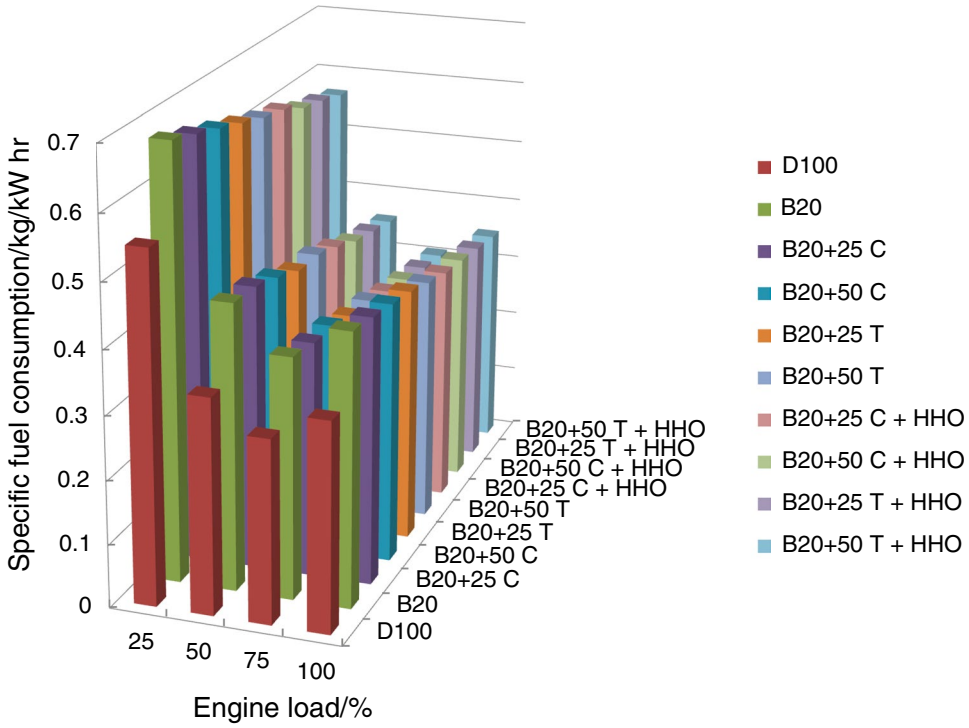

Fig. 6 Fuels' BSFC values at various engine output power

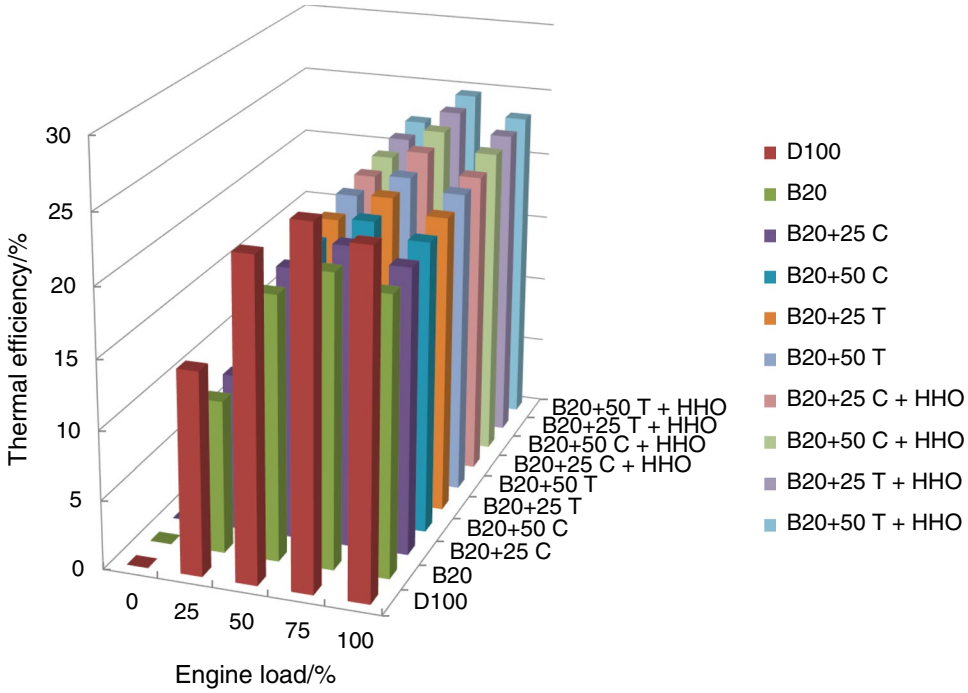

Fig. 7 Nanomaterials and HHO effects on BTE with output power fluctuations

speed and short quenching distance. The biggest decreases in BSFC values were 15% and 20% for B20+50T+HHO and B20+50C+HHO, respectively, as compared to the biodiesel mixture. These findings were corroborated by the literature [7, 21, 23].

Brake thermal efficiency (BTE)

Figure 7 shows the thermal efficiency of burning methyl ester with nanomaterials and hydroxy. Increased fuel consumption and decreased BSFC were associated with higher engine load. Due to its lower calorific value and higher viscosity, methyl ester blend has poor thermal efficiency than crude diesel. Increased viscosity of biodiesel about diesel oil causes insufficient fuel atomization, which produces bigger droplets that hinder ideal burning [50, 51]. Evaporation heat of nanomaterials enhanced the fuel–air mixing, catalytic activity, and heat transfer coefficient. Lower BSFC is the result of improved momentum exchange and heat transfer between fuel molecules relative to the base fuel. Surface area-to-volume ratio improvement was shown due to the presence of nanoparticles. The combustion improvement leads to the enhancement in BTE by achieving complete combustion by secondary atomisation and micro-explosion. The positive impacts of nanoadditions on thermal conductivity and heat transfer rate enhanced the engine's thermal efficiency. During diffusion combustion, BTE rose as the mixture richness was dropped. The oxygen content of the nanoadditive oxide improved the combustion. The diffusive properties and increased flame velocity of HHO gas improve fuel combustion by facilitating fuel injection and air mixing. Brown gas's chemical composition significantly surpassed that of oil due to the interaction between H_2 and O_2 atoms in the subatomic form of hydroxy gas, which improves combustion efficiency without slowing the spread of flame. Remarkably, HHO outperformed all evaluated fuels in terms of flame velocity. The highest enhancements in the thermal efficiency of B20 with HHO and 25 and 50 ppm concentrations of cerium oxide and titanium nanoadditives were shown. The corresponding increases were 14% and 19%. Literature [7, 21, 23] validated these findings.

Exhaust gas temperature (EGT)

Effects of methyl ester blend with different concentrations of cerium and titanium oxides with hydroxy at engine load variation on EGT are shown in Fig. 8. The increase in EGT was caused by the engine load's increased fuel consumption. A shorter premixed phase is a result of higher cetane number in the fuel. The fuel keeps burning until it reaches the expansion stroke, or late combustion stage, which releases more heat and higher exhaust gas temperature [50, 51]. WCO biodiesel blend's exhaust gas temperature was increased in relation to diesel oil because of increased heat loss and reduced thermal efficiency. When nanoparticles were dispersed into B20, the exhaust stream's temperature was dropped. Catalytic oxidation and combustion properties of reactive surfaces were enhanced by the combination of nanomaterials. Enhancements in thermal conductivity,

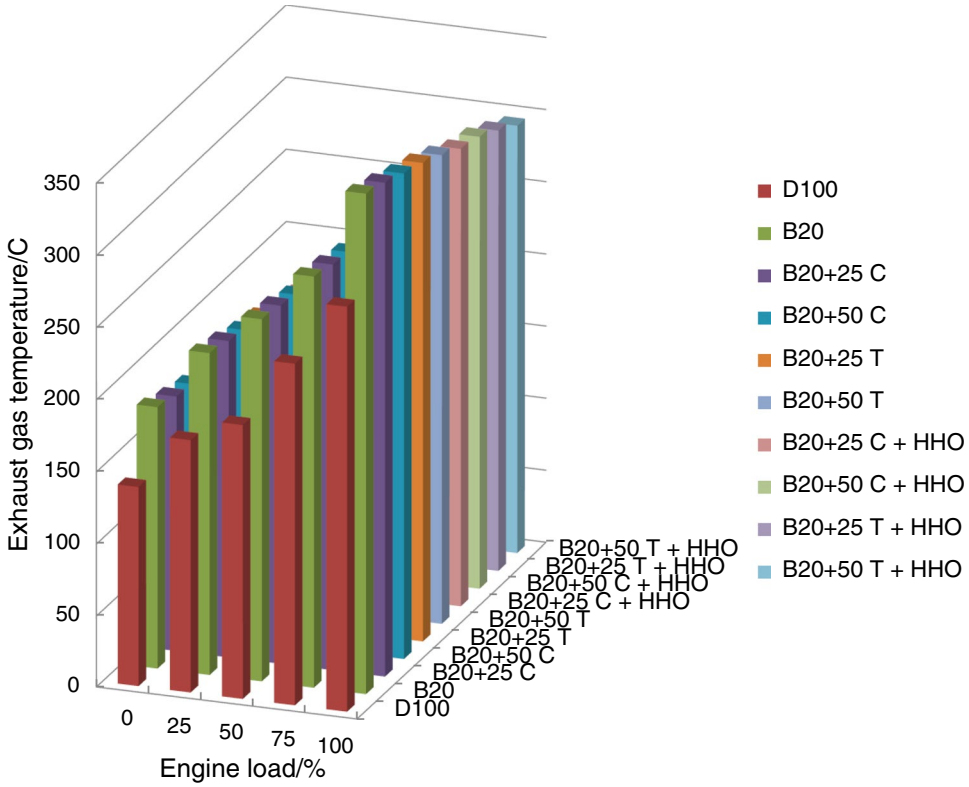

Fig. 8 EGT of the tested blends at engine load change

ignition characteristics, and heat transfer seen when nanoparticles are enriched. Because nanoparticles improve combustion efficiency, their influence lowers the temperature of exhaust gases. By using nanoparticles, the EGT is reduced and the autoignition temperature of the fuel–air mixture is accelerated. Because of their high energy density, nanoparticles reduced exhaust gas temperature and heat loss. Specific fuel consumption was reduced, and thermal efficiency was increased in order to achieve the lower exhaust gas temperature. Due to the diffusion mechanism's diminished capacity to provide a rich mixing zone, EGT was declined. Nanoadditives's oxygen content enhanced combustion and decreased EGT. The lean mixture brought on by HHO and diminished capacity of the diffusion mechanism to create a rich mixing zone were also responsible for the decrease in exhaust temperature. The high oxygen composition and quick flame of hydroxy enhanced combustion, boosting diffusivity and lowering exhaust gas heat loss. When compared to methyl ester combination, the largest reductions in exhaust gas temperature were seen for B20+50T+HHO and B20+50C+HHO, at 12.5% and 17.5%, respectively. These findings were corroborated by the literature [7, 17, 19].

CO emissions

Figure 9 shows carbon monoxide levels for methyl ester blend with CeO_2 and TiO_2 at different loads. Because of the higher fuel consumption and richer air–fuel combination at high output power, CO concentrations rose at high brake power and fell at lower loads. Because biodiesel content of oxygen burns completely, it produces less carbon dioxide than diesel oil. Nanoparticles have shorter igniting delay, more catalytic reactivity, and more surface area contact than base fuels. The concentration of nanoparticles enhanced the combustion and ignition properties. By using nanoparticles, the fuel–air combination quickly achieves the autoignition temperature after the EGT was reduced. Reduced CO emissions are the result of improved fuel oxidation and atomization. Through enhanced evaporation, thermal characteristics, and heat transfer, nanoparticles were able to reduce CO concentrations and shorten ignition delay duration. The increased surface area and chemical reactivity of cerium and titanium oxides were responsible for the larger CO emission reductions. Nanoadditive oxide's oxygen content improved combustion efficiency and reduced CO emissions. Nanoparticles' potent redox activity enables them to transform CO into CO_2. The lean mixture brought on by HHO and diminished capacity of diffusion mechanism to create rich mixing zone were also responsible for the exhaust gas temperature decline. The high oxygen content and quick flame of hydroxy enhanced combustion, boosting diffusivity and lowering exhaust gas heat loss. The greatest decreases in CO emissions of B20 with cerium and titanium oxides of 50 ppm with hydroxy were 13 and 20%, respectively, when related to the crude methyl ester mixture. The same

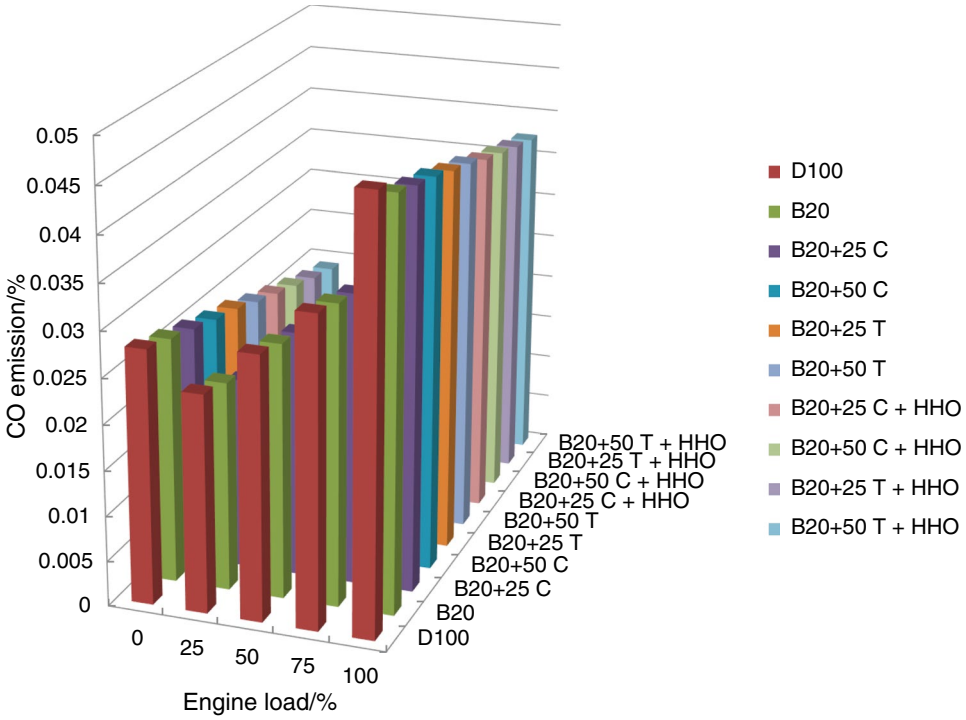

Fig. 9 Influence of nanomaterials on CO at load variations

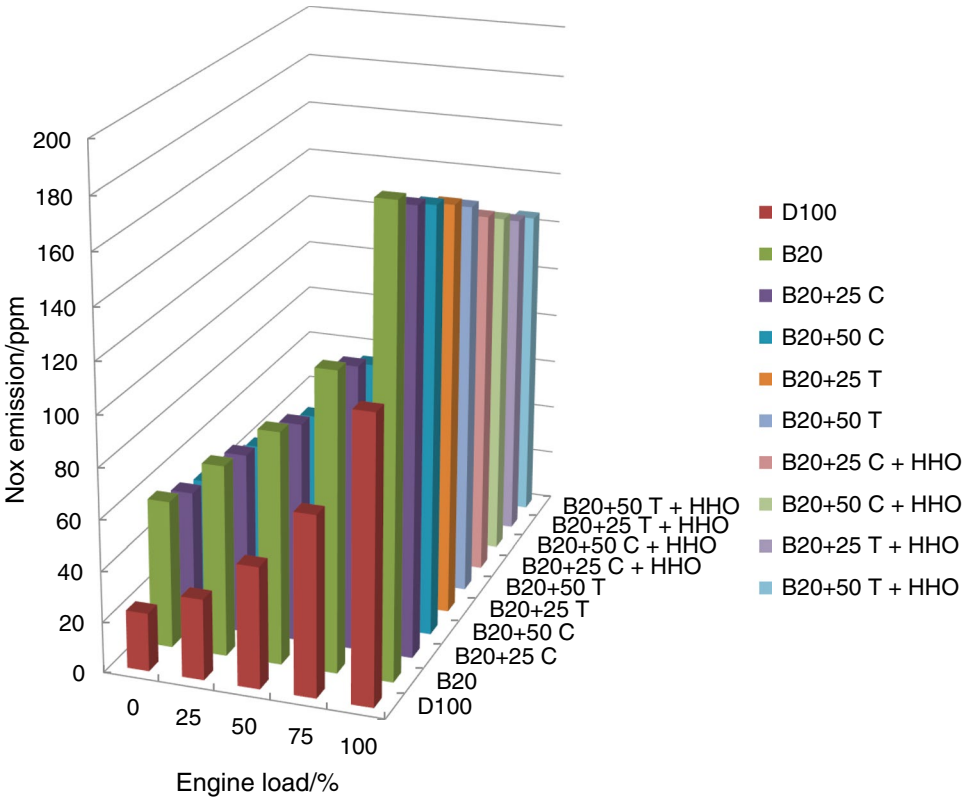

Fig. 10 NOx levels of output power variations using nanoadditives and hydroxy

propensity to add nanoparticles has been demonstrated by other studies [15, 17, 21].

NOx emissions

The impact of adding titanium and cerium oxide to B20 with HHO on NOx emissions is shown in Fig. 10. The drop

in NOx emissions was caused by the drop in exhaust gas temperature. High adiabatic flame temperature, which was linked to the high cylinder temperature, was what led to the increase in NOx emissions. Because of the high fuel–air combination, it increased as engine load increased. When related to diesel oil in B20 blend, the biodiesel's increased oxygen concentration resulted in the increase in NOx emissions. When the biodiesel mixture was exposed to nanoadditive doses of 25 and 50 mg/litre for CeO_2 and TiO_2, the concentrations of nitrogen oxides were reduced. The reduction in NOx emissions is due to improved heat transfer. The nanoparticle acts as an agent that reduces NOx emissions and speeds up evaporation. Better fuel–air mixing, higher catalytic activity, and enhanced thermal conductivity all reduce NOx emissions. A stronger correlation between the hydrocarbon oxidation rate and carbon combustion activation reduced NOx emissions. Using less fuel during the premixed combustion phase results in decreased NOx emissions and lower peak cylinder combustion temperature. The interaction of oxygen and nitrogen atoms which is enabled by the thermal influence of the nanoadditive produced the lowest values of NOx. Application of nanoparticles improved thermal properties, fuel droplet atomization, and combustion. Activity of the nanoparticles accelerated the combustion, producing fine products with the less active radicals and hydrocarbons that thermally decomposed, lowering NOx concentrations. Nitrogen oxide production was reduced due to the improved air fuel mixing rate and air entrainment for nanoadditives to methyl ester blend. Because O_2 and H_2 were present, hydroxy gas burned more efficiently, reducing NOx emissions. NOx emissions were reduced using cooler cylinders and faster hydrogen burn rates. NOx emissions were decreased by the HHO enhanced premixed flame burning and quick flame velocity. It has been demonstrated that using HHO reduces NOx emissions. Brown gas was added to the fuel, which decreased the adiabatic flame temperature and added more air than was required, leading to significant NOx concentrations. Fuel consumption was decreased as a result of the inclusion of HHO. The largest drops in NOx concentrations were seen at 25 and 50 ppm in B20 containing TiO_2 and CeO_2 with HHO, which were 24 and 35% for methyl ester blend B20, respectively. Patterns of NOx emissions were consistent with earlier studies [14, 21, 23].

HC emissions

Figure 11 shows the impact of methyl ester mixture containing nanomaterials on hydrocarbons emissions in diesel engines. High loads produced greater HC concentrations because more fuel was burned and less oxygen was shown. Fuel atomization and fuel–air mixing are affected by shorter ignition durations and higher cetane levels. Biodiesel's increased combustion rate as a result of the bound O_2 in it led to decreased HC values. As a catalyst, nanoparticles sped up the oxidation of hydrocarbons and brought about improved combustion. The nanomaterials' secondary atomization speeds up HC oxidation, which reduces HC emissions. Combustion of carbon deposits and particles reduces

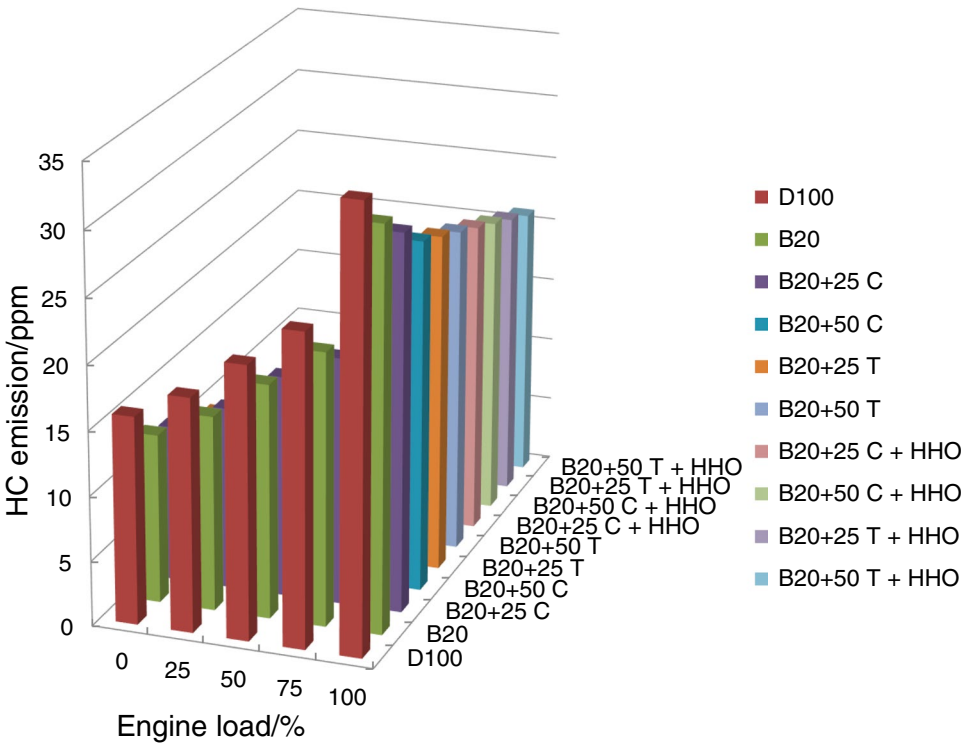

Fig. 11 Effect of fuels containing nanoparticles and hydroxy on HC concentrations

the HC emissions due to the activation energy of nanoparticles on the cylinder wall. Main droplets' micro-explosion results in the decrease in hydrocarbon emissions. The fuel molecules were heated faster and their rate of evaporation increased by the nanoparticles due to the enhanced thermal conductivity of nanoadditives compared to base fuel. HC concentrations declined owing to the nanoparticles' reduction of late combustion and shortening of ignition delay. Due to their higher surface area-to-volume ratios and increased chemical reactivity, CeO_2 and TiO_2 significantly reduced HC emissions. Compared to TiO_2, CeO_2 oxide exhibits improved evaporation rate, thermal conductivities, and heat transfer rate. Nano-oxides' oxygen content improves combustion efficiency and lowers HC concentrations. HC concentrations can be decreased by better fuel oxidation and increased O_2 content from hydroxy in the air intake. Hydrogen's increased flammability extension and shorter quenching distance decreased hydrocarbon concentrations. Higher flame speed and hydrogen diffusivity result in lower HC emissions compared to a non-hydroxy environment. The values of hydrocarbons decreased along with the hydroxy gas's carbon content. The greatest decreases in HC emissions were 25 and 36 percentage for B20+50T+HHO and B20+50C+HHO, respectively, as compared to the crude biodiesel combination. The results from the literature support the trend in HC emissions [7, 9, 23].

Smoke opacity

Smoke emissions of B20 with CeO_2 and TiO_2 nanoparticles with hydroxy are displayed in Fig. 12. The rich air–fuel combination and greater consumption of fuel due to the increased engine load were the reasons for the increase in smoke values. Because the methyl ester mixture has higher cetane number, more oxygen, and shorter ignition delay than diesel oil, it produced less smoke. Fuel–air mixing rate and fuel droplet evaporation were enhanced under the use of nanoparticles which improved thermal conductivity and decreased smoke. Nanoparticles improved thermal properties and combustion due to their reactive surfaces, high surface area-to-volume ratio, catalytic activity, and enhanced heat transfer rate. As the rate of titanium oxide evaporation and heat transfer increased, smoke emissions related to CeO_2 decreased even further. The biodiesel mixture with 50 ppm amounts of titanium and cerium oxide exhibited the largest reductions in smoke in relation to blend of biodiesel. HHO gas's high oxygen content promoted faster and more complete combustion, while its low-carbon content decreased smoke formation and hastened burning when mixed with an biodiesel blend. Better fuel oxidation, increased oxygen concentration, and enhanced combustion were all associated with the addition of hydroxy. In comparison with the methyl ester mixture, the addition of biodiesel blend containing 25 and 50 ppm cerium oxide in combination with HHO produced the most notable reductions in smoke. For CeO_2 and TiO_2 oxides of 50 mg/litre with HHO, the smoke reductions

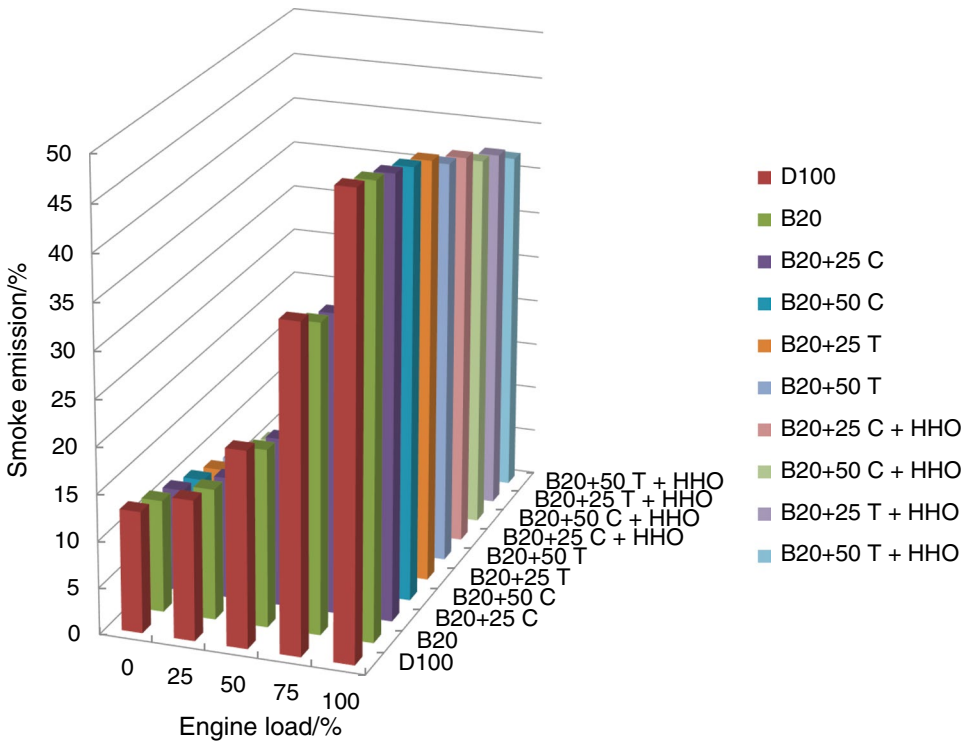

Fig. 12 Smoke values with load change for all fuels

Table 3 Results of MRAE (%) for test samples with different hidden layer size (N_h)

N_h	5		7		10		12	
Parameters	Mean	Std	Mean	Std	Mean	Std	Mean	Std
SFC	10.398	5.143	10.7634	6.2290	21.713	1.388	18.063	3.972
TE	10.299	7.596	12.457	7.897	13.428	6.353	18.170	7.197
EGT	6.535	4.412	5.275	4.343	7.573	1.989	6.360	2.575
CO	13.544	4.462	15.393	5.522	15.866	5.068	15.909	3.626
HC	10.329	3.774	13.786	6.207	16.175	7.601	18.374	8.871
Nox	10.109	10.845	13.918	14.715	16.108	17.706	17.134	10.618
SE	10.599	8.173	16.776	19.967	18.523	17.926	22.483	19.533

Table 4 Correlation coefficient of SFC, TE, EGT, CO, HC, Nox, and SE with input variables: engine load, biodiesel blend, CeO_2, TiO_2, and HHO

Variable	Engine load	*B*	*C*	*T*	HHO
SFC	−0.754	0.165	0.065	−0.082	−0.167
TE	0.881	−0.068	−0.025	0.028	0.054
EGT	0.948	0.182	0.071	−0.070	−0.136
CO	0.799	−0.189	−0.021	−0.194	−0.295
HC	0.808	−0.337	−0.053	−0.281	−0.408
Nox	0.883	0.200	0.070	−0.093	−0.192
SE	0.925	−0.125	−0.006	−0.140	−0.202

Table 5 MAPE and R^2 for SFC, TE, EGT, CO, HC, Nox, and SE

Variable	MAPE,% (Test)	Std	R^2
SFC	2.22	0.55	0.984
TE	2.19	0.61	0.988
EGT	2.92	0.65	0.976
CO	5.16	1.46	0.959
HC	7.81	1.63	0.940
Nox	8.64	2.00	0.955
SE	5.62	1.22	0.985

were 4, 15, and 21% as compared to B20. The findings were confirmed by other studies [15, 19, 21].

Predictive models comparison

This part uses the available experimental data to create ANN and linear regression models that forecast the output parameters: BSFC, BTE, EGT, CO, HC, NOx, and smoke. The following metrics are used to compare the models: This is how the coefficient of determination was computed:

$$R^2(y,\hat{y}) = 1 - \frac{\sum_{i=1}^{N}\left(y_i - \hat{y}_i\right)^2}{\sum_{i=1}^{N}\left(y_i - \bar{y}\right)^2}$$

Table 3 presents the numerical results of MRAE for different N_h. The average of MRAE is calculated over 25 independent computer runs. The ANN model succeeds in getting reasonable values of MRAE, e.g. less than 10%, only for EGT parameter. It is also noticed that standard deviation is at high levels relatively to the average values for all parameters.

To study further the relationship among the seven performance and emission variables and the input fuel characteristics, the correlation coefficient is calculated as illustrated in Table 4.

Although the correlation coefficient only signifies if there is linear relationship between variables, it shows that engine load is the most effective input variable on all seven variables. On the contrary, CeO_2 seems to have the least effect on all variables. This can assert that the TiO_2 nano and HHO are better recommended to use for biodiesel fuels. Mean absolute percentage error (MAPE) and coefficient of determination are shown in Table 5 for all seven variables for the test data only.

According to the results in Table 5, the MAPE errors are all below 10% and reach 2% for SFC, TE, and EGT. This shows that the linear regression model can successfully capture the relationship between variables. By investigating the linear regression , it can be realised that the parameters corresponding to the CeO_2 nanomaterial concentration (for all seven variables) are the least among all coefficients in the same row, emphasising the low impact it has compared to the addition of biodiesel, TiO_2 and HHO. The scatter plot of predicted vs. measured variables for test data in 100 Monte Carlo simulations is shown in Fig. 13a–g. It is shown that using a regression model is fit for the experimental data more than ANN-based models.

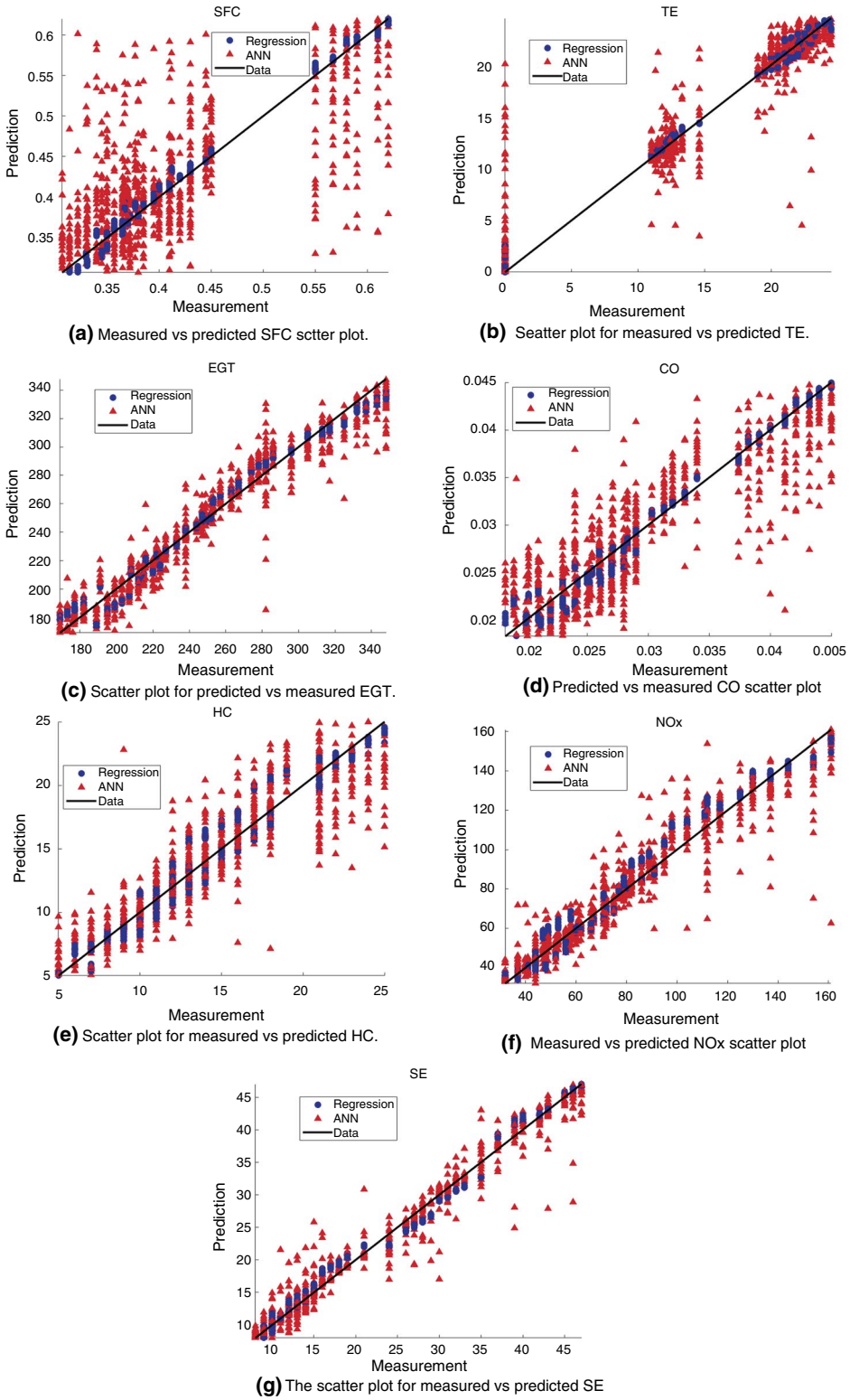

(a) Measured vs predicted SFC scter plot.

(b) Seatter plot for measured vs predicted TE.

(c) Scatter plot for predicted vs measured EGT.

(d) Predicted vs measured CO scatter plot

(e) Scatter plot for measured vs predicted HC.

(f) Measured vs predicted NOx scatter plot

(g) The scatter plot for measured vs predicted SE

Fig. 13 **a** Measured vs. predicted SFC scatter plot. **b** Scatter plot for measured vs. predicted TE. **c**: Scatter plot for predicted vs. measured EGT. **d**: Predicted vs. measured CO scatter plot. **e** Scatter plot for measured vs. predicted HC. **f**: Measured vs. predicted NOx scatter plot. **g**: Scatter plot for measured vs. predicted SE

Conclusions

In this study, methyl eater and diesel oil were combined at 20% by volume to form biodiesel mixture B20. CeO_2 and TiO_2 oxides were added at 25 and 50 mg/litre, respectively. Standards are used to evaluate and agree upon the properties of biodiesel including nanoparticle mixtures. Research is done on the exhaust emissions and engine performance of WCO methyl ester blend with nanoadditions and hydroxy. The output variables were predicted using mathematical

models, including ANN and linear regression. This forecasting uses different loads and fuel mixture combinations based on experimental measurements. The main conclusions were shown.

- At 50 mg/litre with hydroxy, the largest increases in thermal efficiency for biodiesel blend B20 are 14% and 19%, respectively. The biggest BSFC reductions for B20 + 50C + HHO and B20 + 50 T + HHO at maximum output power are 15% and 20%, respectively. In contrast, when B20 waste cooking oil biodiesel blends including 50 mg/litre nanoadditions were examined, the exhaust gas temperature dropped most for TiO_2, CeO_2, and HHO by 12% and 17.5%, respectively.
- CO concentrations fell by 13% and 20%, respectively, when 50 ppm of cerium and titanium oxides were added with hydroxy; however, hydrocarbon emissions decreased by 25% and 36%, respectively. The largest reductions in NOx concentrations at maximum engine brake power are up to 24% and 35% for B20 + 50 T + HHO and B20 + 50C + HHO, respectively, while the largest reductions in smoke emissions are up to 4%, 15%, and 21% for B20.
- Addition of CeO_2 and TiO_2 to WCO combination at a level of 50 ppm results in the improved engine performance and reduced emissions for B20. These nanoadditions may have increased B20's thermal conductivity, heat transfer rate, catalytic reactivity, and evaporation rate. Therefore, in a range of diesel engine applications, it is highly recommended to use biodiesel mixture B20 with 50 ppm nano titanium and cerium oxides with hydroxy.
- In terms of R^2 and MAPE criteria, linear regression and artificial neural network (ANN) models demonstrated remarkable efficacy in forecasting and predicting all engine performance and emission variables; as a result, they can be regarded as a promising option for engine variables prediction and forecasting.

Funding Open access funding provided by The Science, Technology & Innovation Funding Authority (STDF) in cooperation with The Egyptian Knowledge Bank (EKB).

References

1. Mishra S, Chauhan A, Mishra KB. Role of binary and ternary blends of WCO biodiesel on emission reduction in diesel engine. Fuel. 2020;262:116604.
2. Bolaji BO, Adejuyigbe SB. Vehicle emissions and their effects on natural environment-a review. J Ghana Inst Eng. 2006;4:35–41.
3. Wei M, Li S, Xiao H, Guo G. Combustion performance and pollutant emissions analysis using diesel/gasoline/iso-butanol blends in a diesel engine. Energy Convers Manage. 2017;149:381–91.
4. Demirbas A. Importance of biodiesel as transportation fuel. Energy Policy. 2007;35:4661–70.
5. Demirbas A. Progress and recent trends in biodiesel fuels. Energy Convers Manage. 2009;50:14–34.
6. Singh D, Sharma D, Soni SL, Sharma S, Kumar Sharma P, Jhalani A. A review on feedstock's, production processes, and yield for different generations of biodiesel. Fuel. 2020;262:116553.
7. Tamilselvan P, Nallusamy N, Rajkumar S. A comprehensive review on performance, combustion and emission characteristics of biodiesel fueled diesel engines. Renew Sustain Energy Rev. 2017;79:1134–59.
8. Aldhaidhawi M, Chiriac R, Badescu V. Ignition delay, combustion and emission characteristics of Diesel engine fueled with rapeseed biodiesel – a literature review. Renew Sustain Energy Rev. 2017;73:178–86.
9. Soudagar MEM, Nik-Ghazali NN, Abul Kalam M, Badruddin IA, Banapurmath NR, Akram N. The effect of nano-additives in diesel-biodiesel fuel blends: a comprehensive review on stability, engine performance and emission characteristics. Energy Convers Manage. 2018;178:146–77.
10. Hussain F, Soudagar MEM, Afzal A, Mujtaba MA, Fattah IMR, Naik B, et al. Enhancement in combustion, performance, and emission characteristics of a diesel engine fueled with Ce-ZnO nanoparticle additive added to soybean biodiesel blends. Energies. 2020;13:1–20.
11. Mujtaba MA, Masjuki HH, Kalam MA, Noor F, Farooq M, Ong HC, et al. Effect of additivized biodiesel blends on diesel engine performance, emission, tribological characteristics, and lubricant tribology. Energies. 2020;13(13):3375.
12. Örs I, Sarıkoç S, Atabani AE, Ünalan S, Akansu SO. The effects on performance, combustion and emission characteristics of DICI engine fueled with TiO_2 nanoparticles addition in diesel/biodiesel/n-butanol blends. Fuel. 2018;234:177–88.
13. Janakiraman S, Lakshmanan T, Chandran V, Subramani L. Comparative behavior of various nano additives in a DIESEL engine powered by novel Garcinia gummi- gutta biodiesel. J Clean Prod. 2020;45:118940.
14. Dhahad HA, Ali SA, Chaichan MT. Combustion analysis and performance characteristics of compression ignition engines with diesel fuel supplemented with nano-TiO_2 and nano-Al_2O_3. Case Stud Therm Eng. 2020;20:100651.
15. Venu H, Subramani L, Raju VD. Emission reduction in a DI diesel engine using exhaust gas recirculation (EGR) of palm biodiesel blended with TiO_2 nano additives. Renew Energy. 2019;140:245–63.
16. Karthikeyan P, Viswanath G. Effect of titanium oxide nanoparticles in tamanu biodiesel operated in a two cylinder diesel engine. Mater Today Proc. 2020;22:776–80.
17. Örs I, Sarıkoç S, Atabani AE, Ünalan S, Akansu SO. The effects on performance, combustion and emission characteristics of DICI engine fuelled with TiO_2 nanoparticles addition in diesel/biodiesel/nbutanol blends. Fuel. 2018;234:177–88.
18. Praveen A, Rao GLN, Balakrishna B. Performance and emission characteristics of a diesel engine using Calophyllum Inophyllum

biodiesel blends with TiO_2 nanoadditives and EGR. Egypt J Pet. 2018;27:731–8.
19. Yuvarajan D, Babu MD, BeemKumar N, Kishore PA. Experimental investigation on the influence of titanium dioxide nanofluid on emission pattern of biodiesel in a diesel engine. Atmos Pollut Res. 2018;9:47–52.
20. Saxena V, Kumar N, Saxena VK. Multi-objective optimization of modified nanofluid fuel blends at different TiO_2 nanoparticle concentration in diesel engine: experimental assessment and modeling. Appl Energy. 2019;248(248):330–53.
21. Thangaraj S, Govindan N. Evaluating combustion, performance and emission characteristics of diesel engine using karanja oil methyl ester biodiesel blends enriched with HHO gas. Int J Hydrogen Energy. 2018;43:6443–55.
22. Baltacioglua MK, Arat HT, Ozcanli M, Aydin K. Experimental comparison of pure hydrogen and HHO (hydroxy) enriched biodiesel (B10) fuel in a commercial diesel engine'. Int Hydrogen Energy. 2016;41:8347–53.
23. Al-Rousan AA, Musmar SA. Effect of anodes-cathodes inter-distances of HHO fuel cell on gasoline engine performance operating by a blend of HHO'. Int J Hydrogen Energy. 2018;43:19213–21.
24. Baltacioglua MK, Kenanoglu R, Aydın K. HHO enrichment of bio-diesohol fuel blends in a single cylinder diesel engine. Int J Hydrogen Energy. 2019;44:18993–9004.
25. Rimkus A, Matijosius J, Bogdevicius M, Bereczky A, Torok A. An investigation of the efficiency of using O_2 and H_2 (hydrooxile gas -HHO) gas additives in a ci engine operating on diesel fuel and biodiesel. Energy. 2018;152:640–51.
26. Arjun TB, Atul KP, Muraleedharan AP, Albin WP, Bijinraj PB, Arun RA. A review on analysis of HHO gas in IC engines'. Mater Today Proc. 2019;11:1117–29.
27. Nabil T, Khairat Dawood MM. Enabling efficient use of oxy-hydrogen gas (HHO) in selected engineering applications; transportation and sustainable power generation. J Clean Prod. 2019;237:1–14.
28. Ozcanlia M, Akar MA, Calik A, Serin H. Using HHO (Hydroxy) and hydrogen enriched castor oil biodiesel in compression ignition engine. Int J Hydrogen Energy. 2017;42:23366–72.
29. Yilmaz AC, Uludamar E, Aydin K. Effect of hydroxy (HHO) gas addition on performance and exhaust emissions in compression ignition engines. Int J Hydrogen Energy. 2010;35(20):11366–72.
30. Uludamar E, Tosun E, Tuccar G, Yıldızhan S, Calik A, Yıldırım S, et al. Evaluation of vibration characteristics of a hydroxyl)HHO) gas generator installed diesel engine fuelled with different diesel-biodiesel blends'. Int J Hydrogen Energy. 2017;42:23352–60.
31. Subramanian B, Ismail S. Production and use of HHO gas in IC engines. Int J Hydrogen Energy. 2018;43:7140–54.
32. Ismail TM, Ramzy K, Abelwhab MN, Elnaghi BE, Abd El-Salam M, Ismail MI. Performance of hybrid compression ignition engine using hydroxy (HHO) from dry cell. Energy Convers Manage. 2018;155:287–300.
33. Aydin K, Kenanoglu R. Effects of hydrogenation of fossil fuels with hydrogen and hydroxy gas on performance and emissions of internal combustion engines'. Int J Hydrogen Energy. 2018;43:14047–58.
34. Arat HT, Baltacioglu MK, Ozcanli M, Aydin K. Effect of using hydroxy - CNG fuel mixtures in a non-modified diesel engine by substitution of diesel fuel. Int J Hydrogen Energy. 2016;41(19):8354–63.
35. Uludamar E. Effect of hydroxy and hydrogen gas addition on diesel engine fuelled with microalgae biodiesel. Int J Hydrogen Energy. 2018;43:18028–36.
36. Masjuki HH, Ruhul AM, Mustafi NN, Kalam MA, Arbaba MI, Fattah IMR. Study of production optimization and effect of hydroxyl gas on a CI engine performance and emission fueled with biodiesel blends. Int J Hydrogen Energy. 2016;41:14519–28.
37. Jorge M, Matienzo R. Influence of addition of hydrogen produced on board in the performance of a stationary diesel engine. Int J Hydrogen Energy. 2018;43:17889–97.
38. Sakhrieh A, Al-Hares A, Faqes F, Al Baqain A, Alrafie N. Optimization of oxyhydrogen gas flow rate as a supplementary fuel in compression ignition combustion engines. Int J Heat Technol. 2017;35:116–22.
39. Falahat A, Hamdan M, Yamin J. Engine performance powered by a mixture of hydrogen and oxygen fuel obtained from water electrolysis'. Int J Automot Technol. 2014;15:97–101.
40. Ismail T, Ramzy K, Abelwhab M, Elnaghi B, Abd El-Salam M. Performance of hybrid compression ignition engine using hydroxy (HHO) from dry cell. Energy Convers Manag. 2018;155:155–287.
41. Aydin K, Kenanoglu R. Effects of hydrogenation of fossil fuels with hydrogen and hydroxy gas on performance and emissions of internal combustion engines'. Int J Hydrogen Energy. 2018;43:14043–7.
42. Polverino P, D'Aniello F, Arsie I, Pianese C. Study of the energetic needs for the on-board production of oxy-hydrogen as fuel additive in internal combustion engines'. Energy Convers Manag. 2019;179:114–31.
43. Trujillo-Olivares I, Soriano-Moranchel F, Alvarez-Zapata LA, Huerta RGG, Sandoval-Pineda JM. Design of alkaline electrolyser for integration in diesel engines to reduce pollutants emission. Int J Hydrogen Energy. 2019;44:25277–86.
44. Manu PV, Sunil A, Jayaraj S. Experimental investigation using an on-board dry cell electrolyzer in a CI engine working on dual fuel mode. Energy Procedia. 2016;90:209–16.
45. Sharma PK, Sharma D, Soni SL, Jhalani A, Singh D, Sharma S. Characterization of the hydroxy fueled compression ignition engine under dual fuel mode: experimental and numerical simulation. Int J Hydrogen Energy. 2020;45:8067–81.
46. Kenanoglu R, Baltacıoglu MK, Demir MH, M. Ozdemir ME. Performance & emission analysis of HHO enriched dual-fuelled diesel engine with artificial neural network prediction approaches. Int J Hydrogen Energy. 2020;45(49):26357–69.
47. Saravanan N, Nagarajan G. An experimental investigation on a diesel engine with hydrogen fuel injection in intake manifold. SAE Technical Papers 2008; 776–790.
48. Manigandan S, Sarweswaran R, PDevi PB, Sohret Y, Kondratiev A, Venkatesh S. Comparative study of nanoadditives TiO_2, CNT, Al_2O_3, CuO, and CeO_2 on reduction of diesel engine emission operating on hydrogen fuel blends. Fuel. 2020;262:116336.
49. Trujillo-Olivares I, Soriano-Moranchel F, Alvarez-Zapata LA, Gonzalez-Huerta RG, Sandoval-Pineda JM. Design of alkaline electrolyser for integration in diesel engines to reduce pollutants emission. Int J Hydrogen Energy. 2019;44:25277–86.
50. Rajak U, Panchal M, P. Prasanna L, Nagasai C, Ağbulut Ü. Waste to power: experimental investigation and prediction of fuel injection pressure effect on the outputs of DI-CI engine fed by ternary blends using artificial intelligence. J Therm Anal Calorim. 2025;150:12479–99.
51. Babu JPR, Sivarajan C, Prasad BD, Rajak U, Şen Y, Ağbulut Ü. Detailed experimental investigation and optimization of oxygenated diglyme–diesel–n-pentanol ternary blends on compression ignition engine behaviors. J Therm Anal Calorim. 2024;149:13215–32.